

Supporting Information

Murrell and Gardel 10.1073/pnas.1214753109

SI Materials and Methods

Buffers. G-buffer is composed of 2 mM Tris-HCl (pH 8.0) and 0.1 mM CaCl₂, 0.2 mM ATP, 1 mM Sodium Azide, and 0.5 mM DTT. F-buffer is composed of 10 mM Imidazole, 1 mM MgCl₂, 50 mM KCl, 0.2 mM EGTA, and 0.5 mM ATP (pH 7.5). The vesicle buffer is 100 mM NaCl, 20 mM Hepes (pH 7.3). The α -actinin buffer is 20 mM NaCl, 0.1 mM EDTA, 15 mM β -mercaptoethanol, and 20 mM Tris (pH 7.6). The storage buffer for the myosin is 0.5 mM Pipes (pH 7.0) and 0.45 M KCl.

Microscopy. A Nikon Ti inverted microscope with a 60 \times 1.4-Na oil immersion lens (Nikon) and equipped with a spinning-disk confocal (CSUX; Yokagawa) was used. The model cortex is imaged at 491 nm, 568 nm, and 647 nm every 5 s for 15 min on a CCD camera (Coolsnap HQ2; Photometrics) controlled by Metamorph (MDS Analytical Technologies). Photobleaching experiments were performed with a 405-nm laser by a micromirror array that controls local excitation (Mosaic; Photonics Instruments) with a 2-s exposure and a circular region of 20 μ m in diameter.

Sample Chamber. A custom-built sample chamber (Chamlide) consists of two aluminum plates with 17-mm circular holes drilled in their center that sandwich a 25-mm round coverslip and a rubber gasket with an inner diameter of 1.7 cm and thickness of 0.5 cm. This creates an open, circular sample well amenable to high-resolution imaging with dimensions similar to that of the gasket that can hold \sim 1 mL of fluid volume to enable sequential addition of proteins. To prevent evaporation over long times, a 40 \times 50-mm coverslip is overlaid on the top surface of the open chamber.

Preparation of Reconstituted Cortex. Egg phosphatidyl choline (EPC, 91%; Avanti Polar Lipids), nickel lipid [1,2-di-(9Z-octadecenoyl)-sn-glycero-3-([N-(5-amino-1-carboxypentyl)imino-diacetic acid]succinyl) (DGS-NTA), 8.8%; Avanti Polar Lipids], and FITC Green 1,2-Dihexadecanoyl-sn-Glycero-3-Phosphoethanolamine (DHPE) (Molecular Probes; 0.2%) are combined and dried in a glass container under N₂ gas. For simplicity, throughout the text, we do not mention the DHPE when reporting membrane composition as it is used only as a fluorescent reporter. We therefore name only two compositions: 91% EPC/9% NTA and 100% EPC (or “pure EPC”). These compositions are then resuspended by vortexing in vesicle buffer and sonicated in a bath sonicator for upward of 10 min. The resultant small, unilamellar vesicles (SUVs) are added to a 25-mm Piranha-treated coverslip in a custom-built imaging chamber (Chamlide) (\sim 2 mL) for 5 min to fuse and form a fluid bilayer. The membrane is washed and kept hydrated in \sim 500 μ L F-buffer (minus ATP). To bind the actin to the membrane specifically, a truncated, recombinant fimbrin that contains a single actin-binding site, FimA2 [pET-21a-MBP-FimA1A2p-His, gift of Dave Kovar, University of Chicago, Chicago (1)] in ATP-free F-buffer, is added before addition of the F-actin and incubated for 15 min. This His-FimA2 is localized to the surface, using a specific interaction between the nickel lipid and the His-tag on the FimA2 (Fig. S1 A, B, H, and I). The membrane is subsequently washed with ATP-free F-buffer (immediately before addition of actin) with a final volume of \sim 500 μ L.

Stable actin filaments are formed by polymerizing 2.0 μ M dark G-actin [prepared from chicken breast, gift of Yujie Li (University of Chicago, Chicago) and Dave Kovar] and 0.64 μ M Alexa-568 G-actin (Cytoskeleton) mixture in F-buffer supplemented with 0.5% methylcellulose [molecular weight (MW),

14,000], 4.0 μ M dark phalloidin (Cytoskeleton), and 9% glucose oxidase/catalase (Calbiochem) for 2 h on ice. A total of 500 μ L of F-actin is added to the membrane (containing 500 μ L ATP-free F-buffer), such that the final concentration of F-actin is 1.32 μ M and the ATP concentration is 250 nM. The F-actin is allowed to sediment to the surface of the bilayer for a minimum of 15 min such that the accumulation of F-actin approaches a plateau (Fig. S1 C–G and Movie S1). To cross-link the F-actin, a highly concentrated solution of α -actinin (Sigma) is added after the F-actin is crowded to the surface. The α -actinin is allowed to bind the network also for a minimum of 15 min, a time longer than required to associate and bundle the actin network (Fig. S3E). Rabbit skeletal muscle myosin (Cytoskeleton) that has been labeled with Alexa Fluor 647 in myosin storage buffer is then added to a final concentration of 50 nM. As the myosin storage buffer is at 0.45 M KCl, myosin is added as dimers, but assembles thick filaments within minutes when immersed into F-buffer.

The sample chamber volume (1 mL) increases by less than 2% total by the addition of both α -actinin and myosin as they are added in high concentrations. Both α -actinin and myosin are added slowly and in a circular fashion with a 20- μ L pipette tip to the top of the sample volume, directly above the positioned objective. The sample is mixed by exchanging volumes and slow motions with this same, small pipette tip within \sim 5 mm around the objective to not disturb the actin near the bilayer-coated coverslip. As the sample volume is large compared with the mixing volume, this method of mixing prevents disturbance of the F-actin and lipid bilayer. As the α -actinin and myosin dimer are small and diffuse quickly, this method yields homogenous protein concentrations within the actin sheet over length scales much larger than our imaging area (60 \times , \sim 150- μ m diameter viewing area).

Induction of Contraction. In un-cross-linked actin networks ($R_{\text{link}} = 0$), and networks with low concentrations of crosslinker ($R_{\text{link}} = 0.003$), contraction occurs rapidly and heterogeneously throughout the sample after the formation of thick filaments of myosin (Figs. S6 and S8). As the length scale of contraction is small, we can easily visualize the contractile domain and calculate a network strain via methods described below and in Fig. S5. In highly cross-linked ($R_{\text{link}} = 0.03$) samples, however, the length scale of contraction is too large to effectively calculate a strain (Movie S8). We therefore desire to spatially localize the contraction of the network to within the field of view. Before the addition of myosin, we add 40 μ M blebbistatin, which allows for the polymerization and binding of myosin, but inhibits its ATPase activity (Fig. S8 C–F). We then inactivate blebbistatin through the local illumination of the sample with 491 nm light (2), thereby inducing myosin ATPase activity and contraction. Subsequently, we image the F-actin (568 nm) and myosin (647 nm). This process then repeats for all frames in the time course. Spatially controlling the contractility of a highly cross-linked network allows us to assess the buckling and severing of F-actin in a highly cross-linked sample with high accuracy (Fig. S8 C–F). Furthermore, we do this on 100% EPC bilayer to remove all traces of adhesion.

Calculation of F-actin Network and Single F-actin Strain. The x , y , t coordinates of myosin thick filaments were identified by their peak fluorescence in Imaris (Bitplane; Fig. S5A). Individual pairs of thick filaments were chosen opposite the radial zone of contraction. They are separated by an initial distance, w_0 . Over time, this distance will decrease to measure $w(t)$ and the strain is therefore calculated as $\varepsilon_{\text{network}}(t) = 1 - w(t)/w_0$ (Fig. S5 B–D).

Similarly, the end-to-end filament length, L_0 , was measured by hand with ImageJ for each point in time, t . The strain is then calculated from the fractional change in the end-to-end filament length compared with the initial length, $\varepsilon_{\text{filament}}(t) = 1 - L(t)/L_0$.

Calculation of Actomyosin Density in Contractile Zone. A circular region was drawn around the foci that are generated by contraction via Metamorph. The integrated fluorescent actin and myosin intensity that falls within that region is measured as a function of time (ImageJ).

Calculation of Persistence Length. The tangent correlation ($C(s)$) is calculated by taking the mean cosine of the angles ($\theta(s)$) between two segments along an arc length, s . First, the coordinates of the filament are obtained using the ImageJ plugin JFilament. Then, custom-written MATLAB routines are used to calculate $C(s)$ and to fit an “effective” persistence length, ℓ_p , as

$$\langle C(s) \rangle = \langle \cos(\theta(s) - 0) \rangle = e^{-\frac{s}{\ell_p}}. \quad [\text{S1}]$$

$\ell_p(t)$ is calculated for all time points t before and after the formation of myosin thick filaments (Fig. S9).

Determination of Myosin Thick Filament Size, Shape, and Dynamics. Myosin thick filaments are identified as puncta by their local relative intensities and characterized as surface objects, using Imaris (Bitplane). A myosin puncta is an individual object if its fluorescence intensity is significantly higher than background. From the fluorescence intensity, the number of myosin thick filaments (myosin density), average thick filament velocity, thick filament shape (oblate ellipticity), and mean intensities can be calculated as a function of time during contraction (Fig. S4A and B). When overlaid with the strain of the network, the thick filaments finish elongating (minimum in the oblate ellipticity) and then begin to contract (rise in the network strain). During contraction the oblate ellipticity increases again, as thick filaments become round aggregates of myosin. We take the correspondence between the onset of network strain and a minimum in thick filament elongation to mean that myosin adsorption to the F-actin network is minimal past this stage, although we cannot rule out the possibility of minor adsorption of myosin dimers.

The lengths of myosin thick filaments were determined by drawing linescans over deconvolved fluorescence images (Fig. S4C). The linescans are drawn by hand and yield a profile of intensity over space (Fig. S4D). The half-maximum (half-max) width of the linescan is used to determine the width of the myosin thick filaments (Fig. S4E). This yields an average myosin thick filament length of $1.5 \mu\text{m} \pm 0.3 \mu\text{m}$ and constitutes ~ 400 heads per thick filament (3). As a single myosin head has a duty ratio of $\sim 2\%$ under low load, approximately four crossbridges make contact between thick and thin filaments at any given time. If we assume that each motor head contributes force additively, and each motor head can exert 3–4 pN force (4), then the thick filament can exert roughly 12–16 pN of force at low load. As myosin affinity is load dependent, the maximal force exerted could increase under tension up to ~ 600 pN.

Determination of F-Actin Radius of Curvature. The radii of curvature in Fig. 3 are calculated by drawing circular regions along buckling F-actin in ImageJ. From the measured area of the circular regions, the radii are calculated. Only filaments that would have $< 2 \mu\text{m}$ radius of curvature are selected. The radius of curvature in Fig. S10E is calculated by taking the inverse of the curvature, $(d\theta/ds)^{-1}$ of the individual skeletonized F-actin over time.

Calculation of the F-Actin Severing Rate. The severing rate was calculated by identifying individual filaments through segmentation routines in Imaris (Bitplane). Segmented F-actins are

discriminated on the basis of their fluorescence intensity over a background intensity and their separation distance from each other (Fig. S10A). Over time, as filaments sever, there are more segmented objects detected. Subtracting the number of filaments at $t = 0$ (before the formation of myosin thick filaments) from the number of filaments for all subsequent times, t , yields the number of breakage events (as a function of t) due to myosin activity. Normalizing the total number of breakage events by the total length of all filaments before severing yields the number of breaks per micrometer over time. We show that breakage of filaments is due to myosin activity, as the number of filaments remains constant before the addition of myosin (Fig. S10B and Movie S13) but increases after myosin thick filament assembly ($t > 0$, Fig. S10C and Movie S10). The fluctuation in the severing rate before the thick filaments of myosin is due to the error in identifying individual filaments that occurs, for example, when two filaments overlap and are counted as one by the segmentation algorithm.

Severing is attributed to compression if in the image immediately before the severing event (5 s earlier), the F-actin has a radius of curvature below $\sim 5 \mu\text{m}$ (Fig. S10D and E). For straight filaments with immeasurably high radius of curvature, severing is attributed to tension (Fig. S10F). The latter is uncommon, and we estimate the upper limit on severing due to tension compared with all severing events is $\sim 0.2\%$ for ($R_{\text{xlink}} = 0$, $R_{\text{adh}} = 0$) and $\sim 1\%$ for ($R_{\text{xlink}} = 0$, $R_{\text{adh}} = 10$). We discriminate tensile events by visual inspection, counting the number of filaments by hand that appear to fit the aforementioned criteria.

Assessment of F-Actin Bundling. Methylcellulose (MC) (0.2%) is known to induce minor bundling of 3D solutions of elevated concentrations of F-actin (5). Therefore, we wanted to ensure that our 2D, dilute solutions of F-actin ($1 \mu\text{M}$) are filamentous and not significantly bundled in the presence of 0.25% MC. To do so, we quantitatively assessed the extent of bundling in our non-cross-linked network at 0.25% MC ($R_{\text{xlink}} = 0$) and compared this to the bundling observed in a non-cross-linked network ($R_{\text{xlink}} = 0$) at an elevated MC level (0.44%) and a highly cross-linked network ($R_{\text{xlink}} = 0.03$) (Fig. S3A–F). First, we take linescans of the fluorescent F-actin over a region of $\sim 20 \mu\text{m}$. Then, we calculate the average intensity (μ) and SD of the fluorescence intensity (σ) of the F-actin. We then call the quotient, σ/μ , the bundling parameter to assess the amount of bundling that occurs during the sedimentation of an F-actin network at 0.25%, the bundling of the network that occurs as MC is elevated from 0.25% to 0.44%, and the bundling of the network as R_{xlink} is increased from 0 to 0.03 (Fig. S3G). From this calculation, we can see that there is a minimal increase in the bundling parameter as F-actin is sedimented to the surface of a phospholipid bilayer (Fig. S3G, green line). Although the mean F-actin fluorescence intensity increases due to the accumulation of F-actin, its SD does not increase significantly (Fig. S3B). However, bundling is evident both visually (Fig. S3C and E) and quantitatively (Fig. S3D and F) with both elevated concentrations of MC or α -actinin. The bundling that occurs during the elevation of the MC concentration is both due to the effect of bundling of already sedimented F-actin (Fig. S3C, 270 s) and due to the further sedimentation of additional F-actin that remained in solution (Fig. S3C, 570 s). This increase in the bundling of F-actin is also similar to the effect of elevated concentrations of α -actinin (Fig. S3G).

Thus, we estimate that bundling of our non-cross-linked F-actin network in the presence of 0.25% MC is minimal, although we cannot exclude that MC likely has some effect on F-actin/F-actin interactions or promotes small regions of clustered filaments.

Assessment of F-Actin Alignment. Upon the sedimentation of F-actin by 0.25% methylcellulose, filaments have a random local orientation, but align in time as F-actin accumulates (Movie S2). To reduce the alignment of actin, before F-actin addition, we incubate the 91% EPC/9% NTA bilayer in 0.2% BSA for 15 min

before washing it out. Subsequently, the addition of F-actin results in a network with less alignment (Movie S3, 1–2% filaments labeled) than if not treated with BSA. The contraction of this less-aligned F-actin network results in length scales qualitatively similar to those of the contraction of unaligned filaments ($20.5 \pm 3.3 \mu\text{m}$ for BSA-treated membrane and $20.0 \pm 8.8 \mu\text{m}$ for untreated membrane, Movie S6).

Effects of MC on Contraction. To confirm that our experimental conditions were not sensitive to MC concentration, we repeated measurements with 0.15% MC, the minimum concentration required to crowd F-actin to the bilayer surface (Fig. S2), and found qualitatively similar contractility to that in experiments with 0.25% MC (Fig. S7).

SI Text and Equations

The sliding of entangled F-actin well coupled to a fluid bilayer is subject to high drag, both through the viscosity of the membrane and through the viscosity of the surrounding actin solution. We estimate our membrane viscosity is $\sim 1.4 \text{ Pa}\cdot\text{s}$, ~ 500 times the viscosity of the surrounding medium. To pull a $15\text{-}\mu\text{m}$ filament through this viscosity at roughly 150 nm/s (the strain rate of entangled networks) would generate a drag of $\sim 5.2 \text{ pN}$, which is much greater than the force required to buckle it ($\sim 3 \text{ nN}$). This can account for the enhanced severing of a membrane-bound actin network. Furthermore, this is again a lower estimate of the viscosity, as it excludes the contribution from the surrounding filament entanglements that are effectively enhanced by the adhesion itself.

Calculation of Membrane Viscosity. To calculate the diffusivity from the fluorescence recovery after photobleaching (FRAP) data, we use Eq. S2, where w is the radius of the bleached spot, and $t_{1/2}$ is the time it takes to recover half of its integrated intensity (6):

$$D = \frac{w^2}{4t_{1/2}}. \quad [\text{S2}]$$

The measured diffusivity of FITC-DHPE in a primarily EPC bilayer is $D = 3.8 \times 10^{-12} \text{ m}^2/\text{s}$, which is in good agreement with that of Texas Red DHPE in EPC membranes on glass of $1.7 \times 10^{-12} \text{ m}^2/\text{s}$ (7) and Pure EggPC bilayers (4.0×10^{-12}) (8).

FRAP on RFP-His yields a diffusivity of $6.5 \times 10^{-13} \text{ m}^2/\text{s}$. To calculate the membrane viscosity η_m , from the RFP-His [using the radius, r of a GFP barrel of 1.2 nm (9)], we use the Saffman–Delbruck formalism for Stokes Einstein:

$$D(r) = \frac{k_B T}{4\pi\eta_m} \left[\ln\left(\frac{\eta_m}{\eta_w} \frac{1}{r}\right) - \gamma + \frac{1}{2} \right]. \quad [\text{S3}]$$

This yields a 2D membrane viscosity η_m , of $4.5 \times 10^{-9} \text{ N}\cdot\text{s}/\text{m}$. The 3D membrane viscosity is

$$\eta_{3D} = \frac{\eta_m}{h}. \quad [\text{S4}]$$

For a bilayer thickness, $h = 3.3 \text{ nm}$, we get a 3D membrane viscosity of $1.36 \text{ Pa}\cdot\text{s}$. The typical ranges for 3D membrane vis-

cosities are in the range of $3\text{--}151 \text{ Pa}\cdot\text{s}$ (10). This is considerably higher than the viscosity of 0.25% methylcellulose (MW, 14,000) in water ($\sim 2 \text{ mPa}\cdot\text{s}$; Sigma).

Calculation of Drag Force. Using the following equations, we calculate the drag on an individual filament bound to the phospholipid bilayer,

$$D = \mu k_B T \quad [\text{S5}]$$

$$\mu = \frac{v}{F}, \quad [\text{S6}]$$

where μ is the viscous mobility of an individual nickel lipid and D is the diffusivity of the nickel lipid as determined by the FRAP of His-RFP bound to it. This yields a force, $F = 9.5 \times 10^{-16} \text{ N}$ to move a single nickel lipid at 150 nm/s (the rate of contraction). We consider this to be the contribution by an individual lipid molecule to the drag. For an actin filament $15 \mu\text{m}$ in length, there should be a total of 5,454 monomers. As there is an excess of FimA2 to actin, we approximate that every monomer of actin is bound to the surface, and the total force would then be 5.2 pN . This assumes each lipid contributes independently, which is an approximation, as there should be asymmetry in the direction of the applied force. This does not include the resistance due to the F-actin network itself.

Calculation of the Buckling Force. F-actin that is compressed at ends that are free to rotate but not move laterally will buckle under the force given by Eq. S7. For a bending stiffness of $k = 7.3 \times 10^{-26} \text{ N}\cdot\text{m}^2$ (11), and a filament length $L = 0.94 \mu\text{m}$, the corresponding force and energy to buckle are

$$f_b = \frac{\pi^2 k}{L^2} = 0.82 \text{ pN} \quad [\text{S7}]$$

$$E_b = \frac{kL}{2r_c^2} = 3.8 \times 10^{-19} \text{ J}, \quad [\text{S8}]$$

where r_c is the radius of curvature equal to 300 nm . As a single skeletal muscle dimer can exert $\sim 3\text{--}4 \text{ pN}$ of force (4), it can easily buckle an actin filament at the preferred radius of curvature of 300 nm . This corresponds to the measured 0.9 pN and $1.2 \times 10^{-18} \text{ J}$ to bend a single actin filament into a knot with a $0.18\text{-}\mu\text{m}$ radius (12). As we measure contraction for filament lengths longer than $1 \mu\text{m}$, buckling is possible for all realizable filament lengths within this assay.

The force to rupture a filament under tension is as high as 500 pN (13). Taking this over the spacing between actin monomers of 5.3 nm corresponds to an association energy of $2.65 \times 10^{-18} \text{ J}$. Therefore, the energetic cost of bending a single F-actin to 300 nm is less than the cost of rupturing. This is consistent with the nondeterministic severing of F-actin at this radius of curvature, but with its enhanced probability (12).

- Skau CT, Kovar DR (2010) Fimbrin and tropomyosin competition regulates endocytosis and cytokinesis kinetics in fission yeast. *Curr Biol* 20(16):1415–1422.
- Sakamoto T, Limouze J, Combs CA, Straight AF, Sellers JR (2005) Blebbistatin, a myosin II inhibitor, is photoinactivated by blue light. *Biochemistry* 44(2):584–588.
- Morimoto K, Harrington WF (1974) Substructure of the thick filament of vertebrate striated muscle. *J Mol Biol* 83(1):83–97.
- Finer JT, Simmons RM, Spudich JA (1994) Single myosin molecule mechanics: Piconewton forces and nanometre steps. *Nature* 368(6467):113–119.
- Köhler S, Lieleg O, Bausch AR (2008) Rheological characterization of the bundling transition in F-actin solutions induced by methylcellulose. *PLoS ONE* 3(7):e2736.
- Axelrod D, Koppel DE, Schlessinger J, Elson E, Webb WW (1976) Mobility measurement by analysis of fluorescence photobleaching recovery kinetics. *Biophys J* 16(9):1055–1069.
- Hovis JSB, Boxer SG (2001) Patterning and composition arrays of supported lipid bilayers by microcontact printing. *Langmuir* 17:3400–3405.
- Albertorio F, et al. (2005) Fluid and air-stable lipopolymer membranes for biosensor applications. *Langmuir* 21(16):7476–7482.
- Hink MA, et al. (2000) Structural dynamics of green fluorescent protein alone and fused with a single chain Fv protein. *J Biol Chem* 275(23):17556–17560.
- Cicuta P, Keller SL, Veatch SL (2007) Diffusion of liquid domains in lipid bilayer membranes. *J Phys Chem B* 111(13):3328–3331.

11. Gittes F, Mickey B, Nettleton J, Howard J (1993) Flexural rigidity of microtubules and actin filaments measured from thermal fluctuations in shape. *J Cell Biol* 120(4):923–934.
12. Arai Y, et al. (1999) Tying a molecular knot with optical tweezers. *Nature* 399(6735): 446–448.

13. Tsuda Y, Yasutake H, Ishijima A, Yanagida T (1996) Torsional rigidity of single actin filaments and actin-actin bond breaking force under torsion measured directly by in vitro micromanipulation. *Proc Natl Acad Sci USA* 93(23):12937–12942.

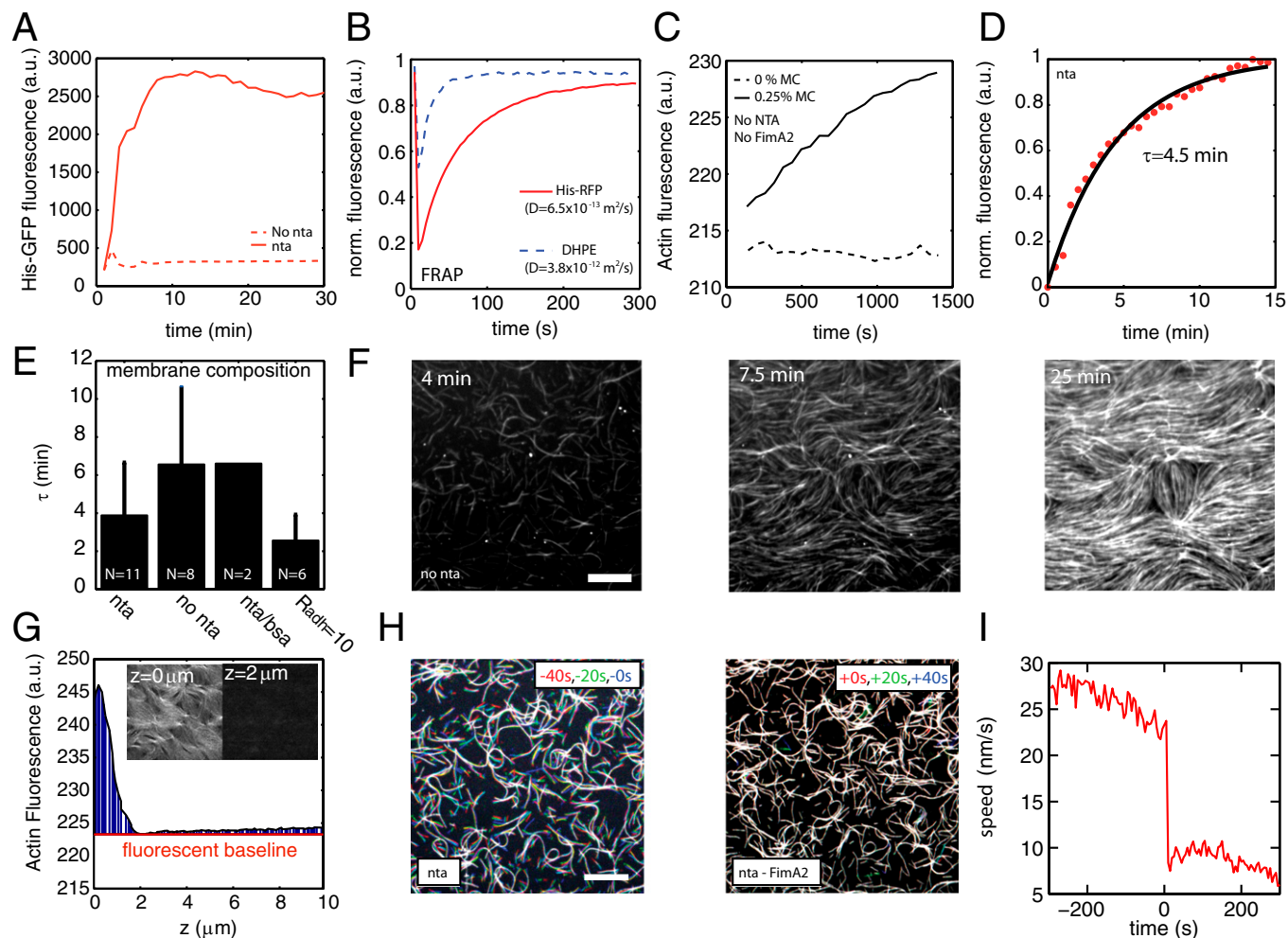


Fig. S1. Localizing proteins to the model membrane by specific and nonspecific interactions. (A) His-tagged green fluorescent protein (His-GFP) intensity at the surface of the supported lipid bilayer as a function of time for 91% EPC/9% NTA membranes (NTA, solid line) vs. 100% EPC membranes (No NTA, dashed line). His-GFP is added at 0 s. (B) Fluorescence recovery after photobleaching (FRAP) experiment of FITC-DHPE (blue line) and His-tagged red fluorescent protein (His-RFP) to measure the mobility of DHPE and NTA lipids, respectively. Bleaching of intensity occurs shortly after 0 s and complete recovery is observed within 300 s. The diffusion coefficient of each species is indicated. (C) Accumulation of F-actin at the surface of a pure EPC phospholipid bilayer by measurement of the intensity of fluorescent actin over time. The addition of 0.25% methylcellulose (MC) crowds F-actin to the surface of the membrane (solid line) but without MC it does not associate to the membrane (dotted line). There is no FimA2 or any other molecule to specifically bind the F-actin present on the bilayer. (D) Normalized mean fluorescence intensity of actin over time (red dots) during accumulation on an EPC/NTA membrane after addition of F-actin at 0 min. The rise time that reflects the dynamics of F-actin accumulation (black line) is fitted with $y = b_1 - b_2 * e^{(-t/\tau)}$. (E) The rise time, t_r , for different compositions of membrane: 91% EPC/ 9% NTA (NTA), 100% EPC (no NTA), and 91% EPC/9% NTA with 15-min 0.2% BSA wash step (NTA/bsa) and with specific adhesion via incubation of 91% EPC/9% NTA membrane with 10 μ M His-FimA2 ($R_{Adh} = 10$). (F) Fluorescence micrographs 4, 7.5, and 25 min after the crowding of F-actin to the surface of a 100% EPC bilayer (no NTA), using 0.25% MC. (Scale bar, 10 μ m.) (G) Mean F-actin fluorescence intensity vs. distance from the phospholipid bilayer (z) as acquired from a confocal z -stack of an F-actin network crowded to the surface of a bilayer with 0.25% MC. (Insets) Fluorescent micrographs of the F-actin network adjacent to the bilayer ($z = 0 \mu$ m) and 2 μ m above the bilayer ($z = 2 \mu$ m). (H, Left) An overlay of F-actin (1–2 μ m labeled) at three successive time points (20-s intervals, in red, blue, and green) before the addition of FimA2 shows high filament mobility. (H, Right) An overlay of three successive time points after addition of FimA2 show drastically reduced filament mobility. Before F-actin sedimentation, the EPC/NTA bilayer is incubated in 0.2% BSA for 15 min. (Scale bar, 10 μ m.) (I) Instantaneous velocity of short (2 μ m) filaments from H. Before the addition of His-FimA2 ($t < 0$), these filaments are highly mobile, but are significantly less mobile after the addition of His-FimA2 at $t = 0$ s.

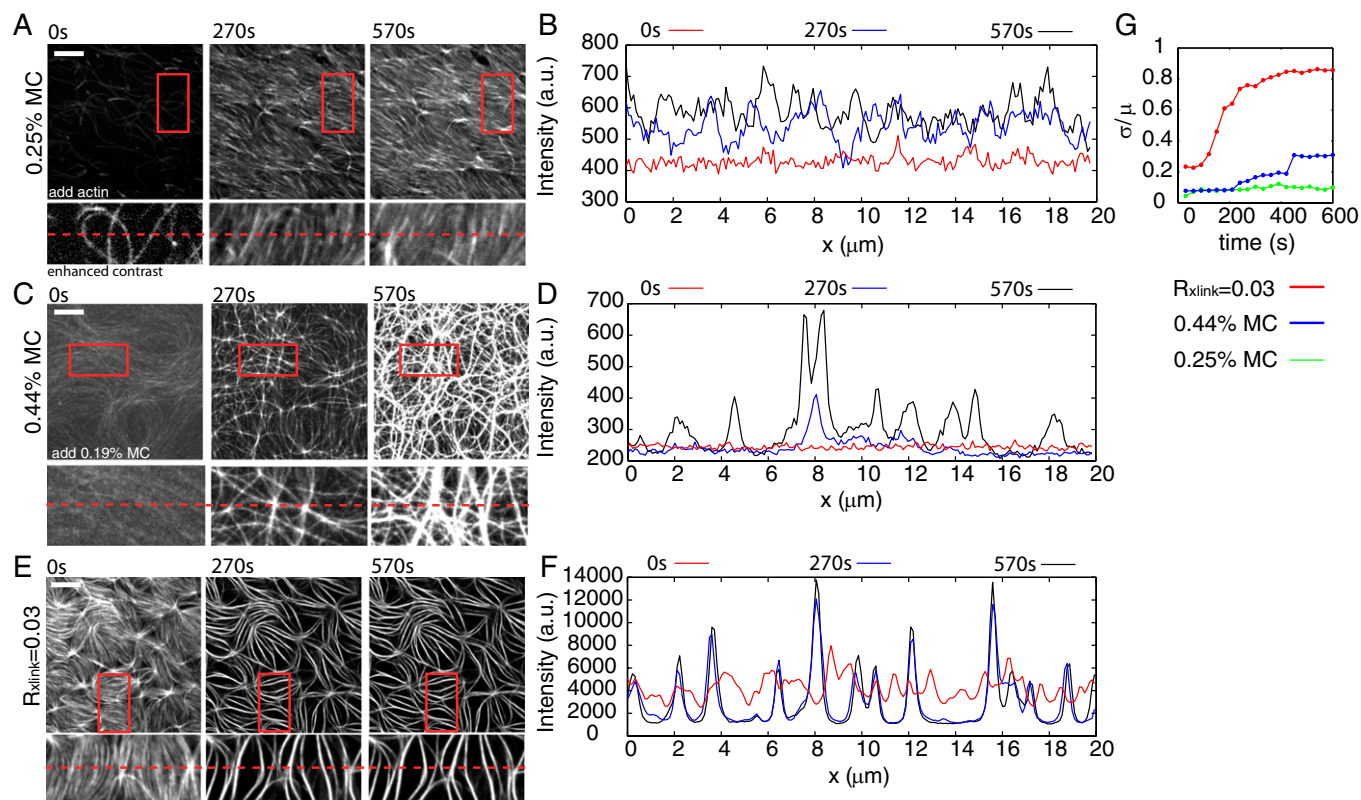


Fig. 53. Effects of MC and α -actinin on forming F-actin bundles. (A) (Upper) Fluorescence micrographs 0 s, 270 s, and 570 s after the crowding of F-actin to the surface of a phospholipid bilayer (91% EPC/9% NTA), using 0.25% methylcellulose (MC) after addition of $1 \mu\text{M}$ fluorescent F-actin at $t = 0$ s. Red rectangle indicates region that is zoomed in and shown in the Lower part. Dotted red line indicates zone used for linescan in B. (C) Zero seconds, 360 s, and 750 s after the increase of MC from 0.25% to 0.44% of an existing F-actin layer. At $t = 0$, the F-actin layer at 0.25% methylcellulose is already present, and additional MC is added to yield a total MC concentration of 0.44%. Dotted red line indicates zone used for linescan in D. (E) Zero seconds, 420 s, and 570 s after the addition of α -actinin (1:30 actin: α -actinin) to an F-actin layer. At $t = 0$, α -actinin is added to an F-actin network at 0.25% MC to yield $R_{xlink} = 0.03$. Dotted red line indicates zone used for linescan in F. (Scale bars: $10 \mu\text{m}$.) (G) Calculation of the SD (σ) divided by the mean (μ) in fluorescence over the linescans in B, D, and F.

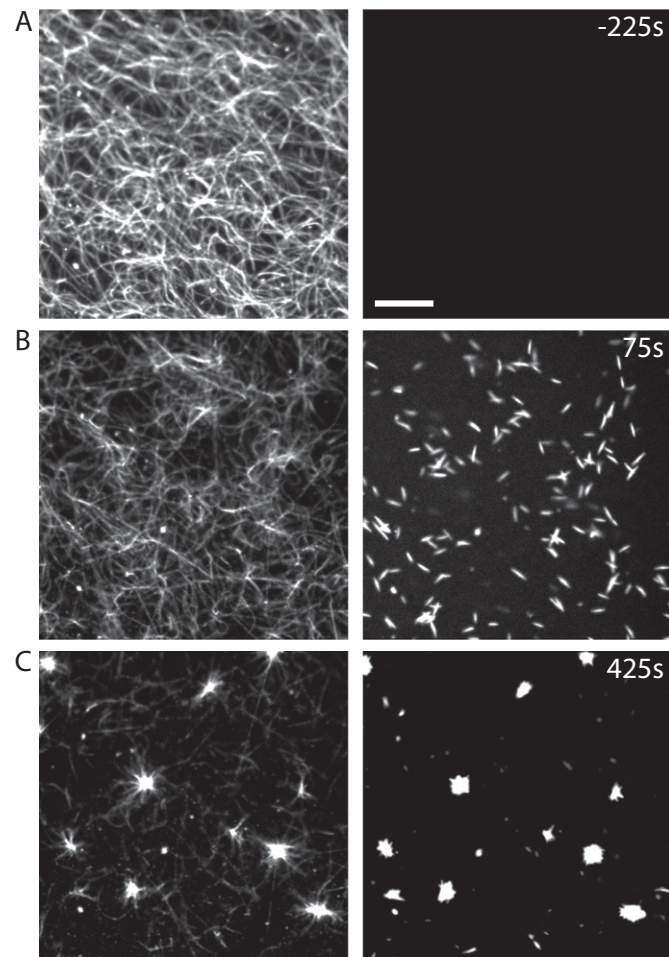
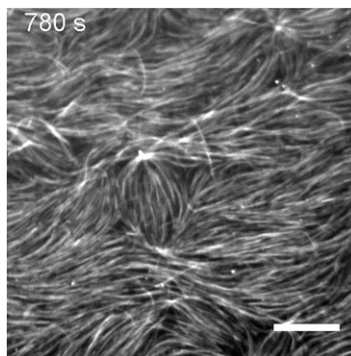
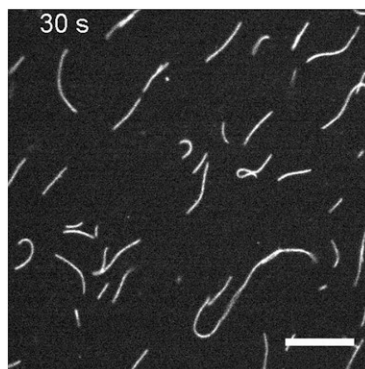


Fig. S7. MC concentration does not qualitatively alter contraction. (*Left*) Images of F-actin (1.32 μM) labeled with Alexa 568 crowded to the surface of a pure EPC bilayer with 0.15% MC. (*Right*) Skeletal muscle myosin II (16.7 nM) labeled with Alexa 647 at (A) $t = -225$ s, (B) 75 s, and (C) 425 s. Myosin thick filaments are fully assembled at $t = 0$ s and contraction is qualitatively consistent with results of Fig. 1, performed at 0.25% MC. (Scale bar, 10 μm .)



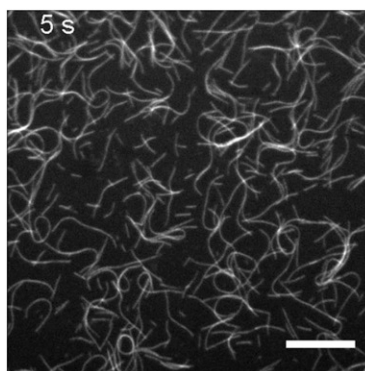
Movie S1. Methylcellulose-induced crowding of F-actin to a bilayer surface. Shown are images of F-actin labeled with Alexa 568 (red) crowded to the surface of a 91% EPC/9% NTA supported bilayer over time. At 0 s, 1.32 μM F-actin is added to buffer containing 0.25% methylcellulose. (Scale bar, 10 μm .)

[Movie S1](#)



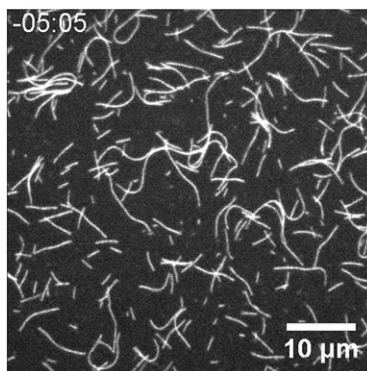
Movie S2. F-actin sedimentation aligns filaments. Shown are images of F-actin labeled with Alexa 568 (0.03 μM) in a network of dark F-actin (1.0 μM), crowded to the surface of a 91% EPC/9% NTA bilayer. One to 2% of the total actin filaments are labeled. At 0 s, F-actin is added to buffer containing 0.25% methylcellulose. (Scale bar, 10 μm .)

[Movie S2](#)



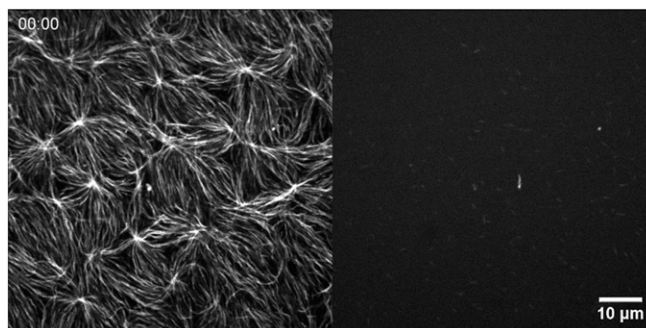
Movie S3. F-actin sedimentation onto BSA-treated bilayer reduces filament alignment. Shown are images of F-actin labeled with Alexa 568 (0.03 μM) in a network of dark F-actin (1.0 μM), crowded to the surface of a 91% EPC/9% NTA phospholipid bilayer that has been incubated in 0.2% BSA for 15 min and subsequently washed. One to 2% of the total actin filaments are labeled. At 0 s, F-actin is added to buffer containing 0.25% methylcellulose. (Scale bar, 10 μm .)

[Movie S3](#)



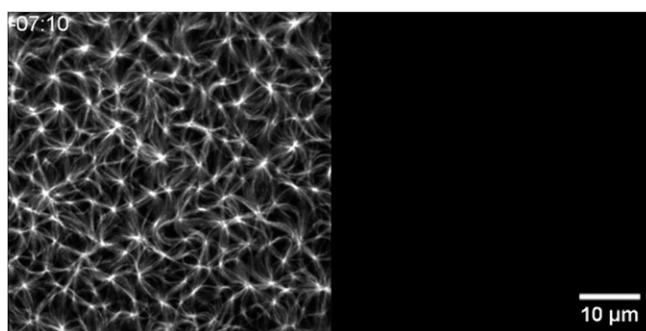
Movie S4. His-FimA2 immobilizes F-actin on the 91% EPC/9% NTA bilayer ($R_{\text{Adh}} = 1,000$). Low concentration ($\sim 0.1 \mu\text{M}$) of F-actin is crowded to the surface by 0.25% MC of a 91% EPC/9% NTA bilayer treated with 0.2% BSA (and subsequently washed). At 00:00, 1 mM His-FimA2 is added to bind individual F-actin to NTA lipid bilayers and, thus, immobilizing them. Time is in mins.

[Movie S4](#)



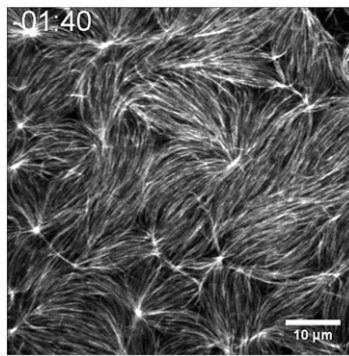
Movie S5. Contraction of un-cross-linked network ($R_{\text{xlink}} = 0$, $R_{\text{Adh}} = 0$). (Left) Images of F-actin ($\sim 1.32 \mu\text{M}$) labeled with Alexa 568 crowded to the surface of 91% EPC/9% NTA bilayer. (Right) Skeletal muscle myosin II (50 nM) labeled with Alexa 647 is added to the network and assembles at $t = 0$ s. Time is in mins.

[Movie S5](#)



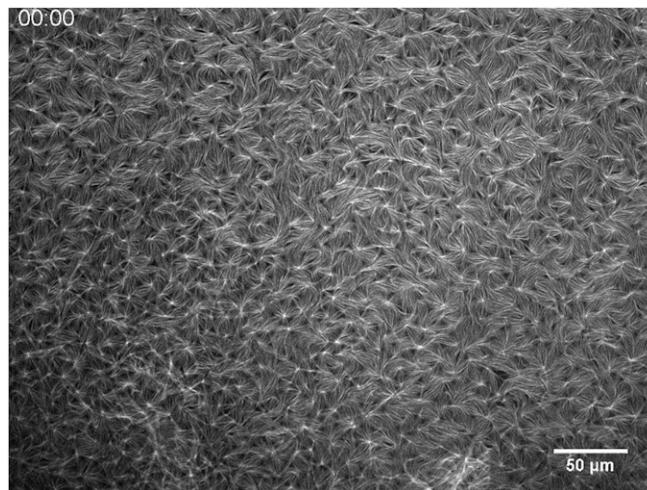
Movie S6. Contraction of an F-actin network with reduced alignment ($R_{\text{xlink}} = 0$, $R_{\text{Adh}} = 0$). (Left) Images of F-actin ($\sim 1.32 \mu\text{M}$) labeled with Alexa 568 crowded to the surface of a 91% EPC/9% NTA bilayer that has been incubated in 0.2% BSA for 15 min and subsequently washed, thereby altering filament organization. (Right) Skeletal muscle myosin II (50 nM) labeled with Alexa 647 is added to the network and polymerizes at $t = 0$ s. Time is in mins.

[Movie S6](#)



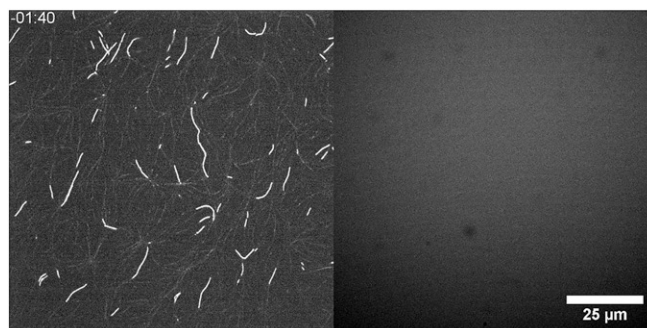
Movie S7. Contraction of isotropically cross-linked networks ($R_{\text{xlink}} = 0.003$, $R_{\text{Adh}} = 0$). Shown are images of F-actin ($\sim 1.32 \mu\text{M}$) labeled with Alexa 568 crowded to the surface of a 91% EPC/9% NTA bilayer, cross-linked with low α -actinin (3 nM, $R_{\text{xlink}} = 0.003$), and then contracted with 50 nM skeletal muscle myosin filaments (not shown for clarity) added at 00:00. Time is in min:s.

[Movie S7](#)



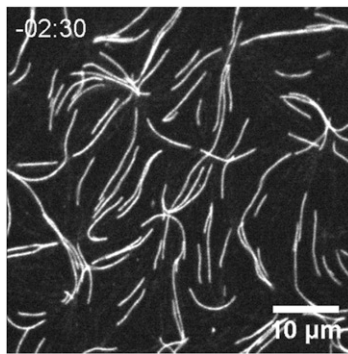
Movie S8. Contraction of bundled networks ($R_{\text{xlink}} = 0.03$, $R_{\text{Adh}} = 0$). Shown are images of F-actin ($\sim 1.32 \mu\text{M}$) labeled with Alexa 568 crowded to the surface of a 100% EPC bilayer and cross-linked and bundled with high concentrations of α -actinin (30 nM, $R_{\text{xlink}} = 0.03$) and then contracted with 50 nM skeletal muscle myosin (not shown for clarity) at 00:00. Time is in min:s.

[Movie S8](#)



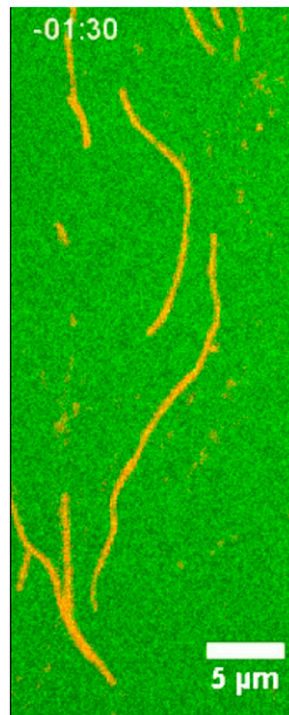
Movie S9. Local contraction of bundled network via blebbistatin (sparsely labeled filaments, $R_{\text{xlink}} = 0.03$, $R_{\text{Adh}} = 0$). (Left) Images of F-actin labeled with Alexa 568 ($0.03 \mu\text{M}$) in a network of dark F-actin ($1.0 \mu\text{M}$), crowded to the surface of a 100% EPC bilayer and cross-linked with 30 nM α -actinin ($R_{\text{xlink}} = 0.03$). Blebbistatin ($40 \mu\text{M}$) was present during the polymerization of the actin. (Right) Thick filaments of 50 nM myosin assemble at 00:00, and upon imaging the region with 491 nm light, the blebbistatin is inactivated and permits local myosin ATPase activity to drive contraction (Fig. S8).

[Movie S9](#)



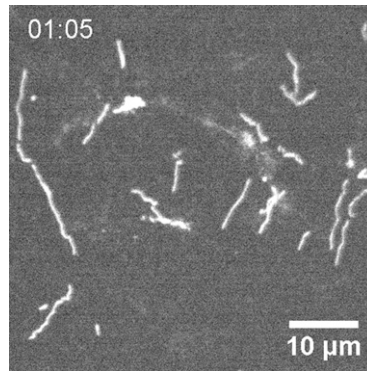
Movie S10. Contraction of un-cross-linked network (sparsely labeled filaments, $R_{\text{link}} = 0$, $R_{\text{Adh}} = 0$). Shown are images of F-actin labeled with Alexa 568 (0.03 μM) in a network of dark F-actin (1.0 μM) and crowded to the surface of a 91% EPC/9% NTA bilayer. The F-actin network is contracted with 50 nM skeletal muscle myosin (not seen), which assembles at 00:00. Time is indicated in min:s.

[Movie S10](#)



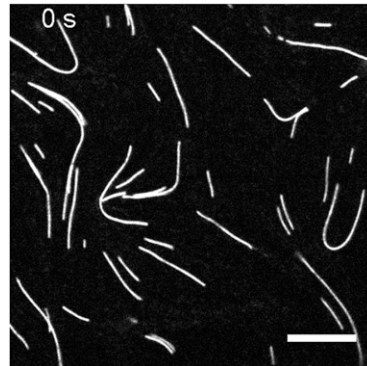
Movie S11. Myosin walking at different rates induces buckling (sparsely labeled filaments, $R_{\text{link}} = 0.003$, $R_{\text{Adh}} = 0$). Shown are images of F-actin ($\sim 1.32 \mu\text{M}$) labeled with Alexa 568 (red) crowded to the surface of a 91% EPC/9% NTA bilayer, cross-linked with low α -actinin (3 nM, $R_{\text{link}} = 0.003$), and then contracted with 50 nM skeletal muscle myosin filaments (green), which assemble at 00:00 (Fig. 2B).

[Movie S11](#)



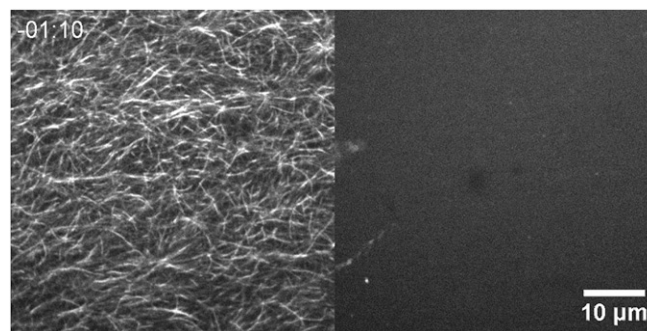
Movie S12. Contraction of adherent network (sparsely labeled filaments, $R_{\text{xlink}} = 0$, $R_{\text{Adh}} = 10$). Shown are images of F-actin labeled with Alexa 568 (0.03 μM) in a network of dark F-actin (1.0 μM) crowded to the surface of a 91% EPC/9% NTA bilayer incubated with 10 μM of His-FimA2 ($R_{\text{Adh}} = 10$). Skeletal muscle myosin II filaments (50 nM) (not shown for clarity) assemble at 00:00. Time is in min:s.

[Movie S12](#)



Movie S13. F-actin does not sever spontaneously due to high exposure. Shown are images of F-actin labeled with Alexa 568 (0.03 μM) in a network of dark F-actin (1.0 μM) and crowded to the surface of a 91% EPC/9% NTA bilayer by 0.25% MC. Images are taken every 5 s for 182 frames (910 s total). (Scale bar, 10 μm .) (Fig. S10B.)

[Movie S13](#)



Movie S14. Contraction of adherent network ($R_{\text{xlink}} = 0$, $R_{\text{Adh}} = 10$). (Left) Images of F-actin ($\sim 1.32 \mu\text{M}$) labeled with Alexa 568 crowded to the surface of a 91% EPC/9% NTA bilayer incubated with 10 μM of His-FimA2 ($R_{\text{Adh}} = 10$). (Right) Skeletal muscle myosin II (50 nM) labeled with Alexa 647 assembles at 00:00. Time is in min:s.

[Movie S14](#)